# CrystEngComm

Accepted Manuscript






ROYAL SOCIETY OF CHEMISTRY

www.rsc.org/crystengcomm

# Hierarchical $Ba_2(B_5O_9)Cl\cdot(H_2O)_{0.5}$ microspheres: surfactant-assisted facile hydrothermal synthesis, $Tb^{3+}$ doping and photoluminescent properties

*Xiuping Chen, Linlin Zhang, Zhaoqiang Zhang, Lin Zhu, Wancheng Zhu*[1],

Department of Chemical Engineering, Qufu Normal University, Shandong 273165, China.

**Abstract:** Three-dimensional hierarchical nanoarchitectures of metal borates self-assembled by one-dimensional or two-dimensional nanostructures have been paid extensive attention for their versatile compositions and excellent performances in various fields. Hilgardite-like metal borates have been widely employed as the nonlinear optical materials and ideal hosts for various luminescent ions. In this contribution, we reported for the first time of a mild surfactant-assisted hydrothermal process for the uniform $Ba_2(B_5O_9)Cl\cdot(H_2O)_{0.5}$ microspheres at 160 ºC for 6.0 h, by using $BaCl_2\cdot 2H_2O$, $H_3BO_3$, and NaOH as raw materials and ethylenediaminetetraacetic acid disodium salt (EDTA-2Na) as the surfactant. The effects of process parameters and the EDTA-2Na assisted formation mechanism were investigated in detail. The as-obtained microspheres exhibited transparent characteristic from ultraviolet to visible range. Within the experimental doping molar percentage of 0-10% in $Ba^{2+}$, the as-prepared $Ba_2(B_5O_9)Cl\cdot(H_2O)_{0.5}$:6%$Tb^{3+}$ phosphors demonstrated strongest PL intensity, revealing the as-obtained $Ba_2(B_5O_9)Cl\cdot(H_2O)_{0.5}$ microspheres of great promising host candidate for emitting luminescent material in light display systems or optoelectronic devices.

**Key words**: $Ba_2(B_5O_9)Cl\cdot(H_2O)_{0.5}$; hierarchical; microspheres; hydrothermal; photoluminescent properties

[1] Corresponding author. Tel.: +86-537-4453130; E-mail: zhuwancheng@tsinghua.org.cn (W. Zhu).

## 1. Introduction

Recently, three-dimensional (3D) hierarchical nanoarchitectures self-assembled by one-dimensional (1D) or two-dimensional (2D) nanostructured building blocks have attracted much concern for their wide applications in catalysis,[1-3] energy storage,[4, 5] sensors,[6, 7] and water treatment,[8, 9] *etc*. owing to the outstanding properties such as unique porous structure, high specific surface area and good mechanical strength. Among varieties of 1D or 2D nanostructures constructed 3D hierarchical nanoarchitectures, metal borates have been paid extensive attention for their versatile compositions and excellent performances in various fields. So far however, there have just only a few of 3D hierarchical alkaline earth metal borates been reported, including flower-like $Mg_3B_2O_6$,[10] hierarchical porous $MgBO_2(OH)$ superstructures,[11] hierarchical laminar rhombic priceite ($Ca_4B_{10}O_{19}\cdot 7H_2O$) superstructures,[12] flower-like and urchin-like $Mg_3B_2O_6$:$Eu^{3+}$,[13] and $LiMnBO_3$ amorphous nanospheres.[14] In addition, hilgardite-like metal borates, such as $M_2B_5O_9X$ (M = Pb, Ca, Sr, Ba, Eu; X = Cl, Br, I, OH)[15-23] and $M_2(B_5O_9)X\cdot Y(H_2O)$ (M = Pb, Ca, Ba; X = Cl, OH; Y=0.5, 1)[24-29] containing both $BO_3$ triangles and $BO_4$ tetrahedra within the structure and thus exhibiting more complex boron-oxygen groups, have also been synthesized as the nonlinear optical materials (NLO), which are widely employed in various fields based on their unique properties. Also as known, the fluorescent materials synthesized by the matrix borates have attracted worldwide attention as a result of the simple process, low cost, high fluorescence intensity and excellent mechanical properties. Besides, the hilgardite-like metal borates containing the tetrahedral borate group $BO_4$ have been confirmed as ideal hosts for various luminescent ions.[30]

Currently, hilgardite-like structures are generally synthesized by high temperature chemical vapor deposition (CVD),[30, 31] molten salt synthesis (MSS)[16, 20, 32] or relatively rigorously hydrothermal route[24, 28, 29]. For example, $Ba_2B_5O_9Cl$ whiskers (diameter: 0.4-1.0 μm, length: 10-25 μm) were synthesized by the MSS method at *ca.* 700 ºC for 8.0 h.[20] Colorless transparent single crystals of $Ba_2[B_5O_9]Cl\cdot 0.5H_2O$ were obtained by using a hydrothermal

systems of ACl ($A_2CO_3$)-BaO-$B_2O_3$-$H_2O$ (A=Li, Na, K, Rb, Cs, $NH_4$ cations) at T=277 ºC / P=100-150 bar for 20-25 days.[24] Single crystals of the $Ba_2[B_5O_9]Cl{\cdot}0.5H_2O$ compounds were prepared in the hydrothermal barium borate system at T=270-280 ºC / P=100 atm for 18-20 days.[29] Thus, although high temperature based techniques can easily produce high crystallinity crystals, the inevitably accompanied problems such as high temperature,[31, 32] high energy consumption,[16] and some cases requisite reducing atmosphere,[32] long reaction time, or mass use of flux agent, *etc.* will in turn greatly restrict the practical employment of these techniques. In contrast with CVD or MSS, mild hydrothermal technology has been widely recognized as a promising alternative route to advanced functional materials for its distinct advantages (e.g. high purity of product, good uniformity, narrow particle size distribution, low energy consumption, *etc.*).[8, 33, 34] It still remains a huge challenge to realize controllable preferential growth of the 1D or 2D nanostructured building blocks as well as further self-assembly for 3D hierarchical nanoarchitectures of hilgardite-like metal borates.

Herein, we reported for the first time of a mild and controllable surfactant-assisted hydrothermal process for the uniform $Ba_2(B_5O_9)Cl{\cdot}(H_2O)_{0.5}$ microspheres at 160 ºC for 6.0 h, by using $BaCl_2{\cdot}2H_2O$, $H_3BO_3$, and NaOH as raw materials and EDTA-2Na as the surfactant. Meanwhile, the effects of process parameters on the hydrothermal products as well as the EDTA-2Na assisted formation mechanism were discussed. Moreover, $Ba_2(B_5O_9)Cl{\cdot}(H_2O)_{0.5}{:}xTb^{3+}$ phosphors were obtained via $Tb^{3+}$ doping, which confirmed the as-obtained $Ba_2(B_5O_9)Cl{\cdot}(H_2O)_{0.5}$ microspheres as great potential host for emitting luminescent material. This deepened the understanding of the crystal growth and self-assembly and also enlarged the future applications of the 3D hierarchical nanoarchitectures of hilgardite-like metal borates in related fields.

## 2.Experimental

### 2.1 Synthesis of the hierarchical $Ba_2(B_5O_9)Cl{\cdot}(H_2O)_{0.5}$ microspheres

All reagents were analytical grade and used directly without further purification. In a typical procedure, 1.855 g of $H_3BO_3$, 0.600 g of NaOH and 3.664 g of $BaCl_2 \cdot 2H_2O$ (molar ratio: Ba:B:OH=1:2:1) were dissolved into 20.0, 10.0 and 18.0 mL of deionized (DI) water, respectively. The NaOH solution, 0.150 g of EDTA-2Na powder and $BaCl_2$ solution was successively added into the $H_3BO_3$ solution under vigorous magnetic stirring at room temperature. The resultant slurry was transferred into a Teflon-lined stainless steel autoclave with a capacity of 61.0 ml. The autoclave was sealed, heated to 160 ºC (heating rate: 5 ºC $min^{-1}$), kept in an isothermal state for 6.0 h, and then cooled down to room temperature naturally. The product was collected, washed with DI water and ethanol for three times, and then dried at 60 ºC for 12.0 h. To evaluate the effects of the process parameters on the hydrothermal product, the reactant temperature, time, concentration and amount of EDTA-2Na were tuned within the range of 4.196-16.790 mmol $L^{-1}$ respectively, with other conditions unchanged.

### 2.2 Preparation of the $Ba_2(B_5O_9)Cl \cdot (H_2O)_{0.5}:xTb^{3+}$ phosphors

Based on the synthesis of the hierarchical $Ba_2(B_5O_9)Cl \cdot (H_2O)_{0.5}$ microspheres, various amount of $Tb^{3+}$ ions doped microspheres ($Ba_2(B_5O_9)Cl \cdot (H_2O)_{0.5}:Tb^{3+}$) were prepared, showing distinct luminescent properties. Typically, 1.855 g of $H_3BO_3$, 0.600g of NaOH and 3.664 g of $BaCl_2 \cdot 2H_2O$ (molar ratio: Ba:B:OH=1:2:1) were dissolved into 20.0, 10.0 and 18.0 mL of DI water, respectively. Then NaOH solution, 0.150 g of EDTA-2Na powder, 0.408 g of $Tb(NO_3)_3 \cdot 6H_2O$ powder and $BaCl_2$ solution was added into the $H_3BO_3$ solution under magnetic stirring at room temperature successively, with the molar percentage of $Tb^{3+}$ in $Ba^{2+}$ as 6%. The resultant slurry was transferred into a Teflon-lined stainless steel autoclave with a capacity of 61.0 ml. The autoclave was sealed and heated to 160 ºC for 6.0 h (heating rate of 5 ºC $min^{-1}$) and cooled down to room temperature naturally. The product was filtered, washed with DI water and ethanol for three times, and then dried at 60 ºC for 12.0 h. To explore the effects of doping amount on the luminescent properties, a series of $Ba_2(B_5O_9)Cl \cdot (H_2O)_{0.5}:xTb^{3+}$ phosphors were synthesized via tuning the doping amount of x within the range of 0-10%, with other conditions kept the same.

### 2.3 Characterization

The crystal structure of the samples was identified by an X-ray powder diffractometer (XRD, MiniFlex600, Rigaku, Japan) with a Cu-$K_\alpha$ radiation ($\lambda$ = 1.5406 Å) and a fixed power source (30 kV, 10.0 mA). The morphology and microstructure of the samples were examined using a field emission scanning electron microscope (SEM, JSM 7401F, JEOL, Japan, at 3.0 kV), and a high resolution transmission electron microscopy (TEM, JEM-2010, JEOL, Japan). Size distribution of the microspheres was estimated by direct measuring *ca.* 100 particles from the typical SEM images. The measurements of photoluminescence (PL) and photoluminescence excitation (PLE) spectra were carried out using a fluorescence spectrophotometer (HITACHI F-4600, Japan) equipped with a 150 W xenon lamp as the excitation light source. The chemical bonds in the molecules on the hydrothermal product were determined by the Fourier transform infrared spectrum (FT-IR, Nexus 470, Nicolet, USA). The absorbance was determined using a UV-visspectrophotometer (UV-756 CRT, Shanghai Yoke Instrument and Meter Co., LTD, China).

## 3.Results and discussion

### 3.1 Hydrothermal synthesis of the $Ba_2(B_5O_9)Cl\cdot(H_2O)_{0.5}$ microspheres

Composition, morphology, and chemical bond related information of the hydrothermal product obtained at 160 ºC for 6.0 h with a molar ratio of Ba:B:OH as 1:2:1 and reactant concentration of $BaCl_2$ as 0.313 mol $L^{-1}$, were evaluated by XRD pattern, SEM/TEM images, and FT-IR spectrum, as shown in **Fig. 1.** The XRD pattern of the hydrothermal product was well indexed to the pure phase of orthorhombic $Ba_2(B_5O_9)Cl\cdot(H_2O)_{0.5}$ (**Fig. 1(a)**, JCPDS No. 70-3930, a = 11.716 Å, b = 11.574 Å, c = 6.7 Å, $\alpha$ = 90º, $\beta$ = 90º, $\gamma$ = 90º and space group of Pnn2(34)), with distinct uniform spherical morphology (**Fig. 1(b)**). The high magnification SEM image shows that the typical hydrothermally synthesized microspheres consisted of one dimensional (1D) nanorods (**Fig. 1($b_1$)**), with a length of 0.4-1.4 μm and a diameter of 40-240 nm. And the statistical data also reveals that *ca.* 97% of the as-synthesized

microspheres had a diameter within the range of 3.0-5.0 μm (**Fig. 1($b_2$)**), confirming the narrow size distribution of the uniform microspheres. The TEM image shows that the constitutional nanorods exhibited distinct straight rod-like shape with smooth surface (**Fig. 1(c)**). The interplanar spacings of 0.577 nm detected from the legible lattice fringes, which were recorded from the orange rectangular region (**Fig. 1(c)**) and along the longitudinal direction of the nanorod (**Fig. 1($c_1$)**) are quite similar to the standard value (0.582 nm) of the (101) planes, indicating the preferential growth of the nanorod-like sub-units parallel to the (101) planes. The high resolution TEM image reconfirmed the high crystallinity of the as-synthesized microspheres, in accordance with the XRD result (**Fig. 1(a)**). In contrast, the low magnification TEM image again demonstrates the spherical morphology of the microspheres on the one hand, and also clearly reveals that the microspheres were constituted of nanorods on the other hand (**Fig. 1($c_2$)**). Both the high magnification SEM image (**Fig. 1($b_1$)**) and TEM image (**Fig. 1($c_2$)**) indicate that the sub-units of the as-synthesized microspheres, or constitutional nanorods, were closely interlinked with each other, leading to the as-obtained microspheres.

**Fig. 1(d)** demonstrates the FT-IR spectrum of the $Ba_2(B_5O_9)Cl\cdot(H_2O)_{0.5}$ microspheres. According to the FT-IR spectroscopic study on borates,[35] the band at 3428 $cm^{-1}$ was due to the O-H stretching of the absorbed water. The band at 1630 $cm^{-1}$ was attributed to the H-O-H bending of the lattice water. The bands in the frequency range 1462-1307 $cm^{-1}$ and band at 1077 $cm^{-1}$ were owing to the asymmetric stretching of $B_{(3)}$-O. The band at 915 $cm^{-1}$ was corresponded to the symmetric stretching of $B_{(3)}$-O. The band at 1265 $cm^{-1}$ was ascribed to the in-plane bending of B-O-H. The bands in the frequency range 992-962 $cm^{-1}$ and 853-759 $cm^{-1}$ could be assigned to the asymmetric and symmetric stretching of $B_{(4)}$-O, respectively. Besides, the out-of-plane bending of $B_{(3)}$-O were reflected in the range from 730-635 $cm^{-1}$. These FT-IR results somehow further confirmed the composition of the products, similar to the previously reported results.[19]

### 3.2 Effect of reactant concentration on the hydrothermal products

**Fig. 2** shows the variation of the composition and morphology of the hydrothermal products via tuning the reactant concentration of $BaCl_2$ within the range of 0.104-0.626 mol $L^{-1}$ whereas with other conditions kept the same. As shown, all products were confirmed as pure phase of $Ba_2(B_5O_9)Cl\cdot(H_2O)_{0.5}$ within the experimental range of concentration (**Fig. 2(a)**). When the concentration of $BaCl_2$ was 0.104 mol $L^{-1}$, the hydrothermal product was distinct rod-like or rare cubic-like $Ba_2(B_5O_9)Cl\cdot(H_2O)_{0.5}$ (**Fig. 2($a_1$, b)**). With the concentration increasing to 0.209 mol $L^{-1}$, the product was confirmed as irregular $Ba_2(B_5O_9)Cl\cdot(H_2O)_{0.5}$ assemblies consisted of microrods (**Fig. 2($a_2$, c)**). In contrast, as the concentration was increased to 0.626 mol $L^{-1}$, the hydrothermal product turned to $Ba_2(B_5O_9)Cl\cdot(H_2O)_{0.5}$ microspheres with non-uniform diameters, accompanied by sparse disassembled microrods and cubic or irregular plate-like particles (**Fig. 2($a_3$, d)**). The low degree of supersaturation derived from low reactant concentration was believed to be responsible for the formation of the 1D microrods, whereas high degree of supersaturation originated from high reactant concentration favored the 3D growth or self-assembly of the microspheres.[36-38] Apparently, this indicated the optimum concentration of $BaCl_2$ for the formation of uniform $Ba_2(B_5O_9)Cl\cdot(H_2O)_{0.5}$ microspheres of 0.313 mol $L^{-1}$, as demonstrated in **Fig. 1**.

### 3.3 Effect of temperature and time on the hydrothermal products

To understand the hydrothermal growth of the $Ba_2(B_5O_9)Cl\cdot(H_2O)_{0.5}$ microspheres, time and temperature dependent experiments were carried out. After the introduction of $BaCl_2$, the resultant precipitate within the slurry was confirmed as tiny quasi-spherical amorphous nanoparticles (NPs), as shown in **Fig. 3($a_1$, b)**. When hydrothermally treated at 130 ºC for 3.0 h, bigger amorphous NPs were obtained (**Fig. 3($a_2$, c)**). When treated at 130 ºC for 6.0 h, distinct low crystallinity and relatively loose $Ba_2(B_5O_9)Cl\cdot(H_2O)_{0.5}$ microspheres with a diameter of *ca.* 10.0 μm emerged, and the microspheres were obviously assembled by multitudes of tiny NPs (**Fig. 3($a_3$, d)**). When treated

at 160 ºC for 1.0 h, the crystallinity of the $Ba_2(B_5O_9)Cl\cdot(H_2O)_{0.5}$ microspheres became higher. Simultaneously, the surfaces of the microspheres exhibited ravines, and short rod-like sub-units appeared (**Fig. 3($a_4$, e)**). When treated at 160 ºC for 3.0 h, distinct $Ba_2(B_5O_9)Cl\cdot(H_2O)_{0.5}$ microspheres were acquired (**Fig. 3($a_4$, f)**), 92% of which were with a diameter ranging from 5.0 to 7.0 μm (**Fig. 3($f_1$)**). This was larger than those uniform $Ba_2(B_5O_9)Cl\cdot(H_2O)_{0.5}$ microspheres containing longer nanorods acquired at 160 ºC for 6.0 h (**Fig. 1(b)**) with a diameter of 3.0-5.0 μm and much narrower diameter distribution (**Fig. 1($b_2$)**). Nevertheless, when the hydrothermal time was further prolonged to 12.0 or 18.0 h at 160 ºC, unknown phase of impurities emerged in addition to the main phase of $Ba_2(B_5O_9)Cl\cdot(H_2O)_{0.5}$. With the hydrothermal time going on, the relative diffraction intensity of the unknown phase tended to be higher (**Fig. S1($a_1$-$a_2$)**), indicating the increasing in the amount of the impurites. Mean while, some irregular particles (**Fig. S1(b)**) and even bulky plates (**Fig. S1(c)**) were formed.

### 3.4 Effect of EDTA-2Na on the hydrothermal product

To get deeper insight into the formation of the microspheres, the effect of EDTA-2Na on the hydrotheraml product obtained at 160 ºC for 6.0 h (molar ratio of Ba:B:OH = 1:2:1, reactant concentration of $BaCl_2$ = 0.313 mol $L^{-1}$) was investigated, as shown in **Fig. 4**. It could be seen that, the hydrothermal products were all consisted of pure phase of $Ba_2(B_5O_9)Cl\cdot(H_2O)_{0.5}$ with or without EDTA-2Na, and the crystallinity of the product got a little weaker with the increase in the amount of EDTA-2Na from 0.0 to 16.790 mmol $L^{-1}$ (**Fig. 4($a_1$-$a_3$)**). Notably however, the morphology varied with each other significantly. Without the assistance of EDTA-2Na, nanorods or irregular aggregates randomly constructed by nanorods were formed (**Fig. 4(b)**). With the introduction of 2.798 mmol $L^{-1}$ of EDTA-2Na, nanorods and distinct microspheres constituted of nanorods emerged (**Fig. 4(c)**). When the amount of EDTA-2Na was increased to 8.395 mmol $L^{-1}$, the uniform $Ba_2(B_5O_9)Cl\cdot(H_2O)_{0.5}$ microspheres with narrow size distribution were obtained (**Fig. 1**). If the amount of EDTA-2Na was further doubled to 16.790 mmol $L^{-1}$, more microspheres were acquired whereas the size distribution of the microspheres became broader, and 90% of the

microspheres had a diameter within the range of 3.0-6.0 μm. Apparently, the surfactant EDTA-2Na affected the crystallinity and especially the morphology of the products.

### 3.5 EDTA-2Na assisted formation mechanism of $Ba_2(B_5O_9)Cl\cdot(H_2O)_{0.5}$ microspheres

Based on the effect of temperature and time as well as EDTA-2Na on the evolution of composition and morphology of the product, formation of the hierarchical $Ba_2(B_5O_9)Cl\cdot(H_2O)_{0.5}$ microspheres could thus be figured out. From a chemical point of view, the dissolution of $H_3BO_3$, NaOH and EDTA-2Na led to corresponding aqueous ions first, demonstrated as eq. (1-3). With the introduction of $BaCl_2$, the EDTA-$^{2-}$ ions could immediately chelate the newly dissociated $Ba^{2+}$ ions, resulting in the chelate EDTA-Ba (complex) due to the strong chelation between $Ba^{2+}$ and EDTA-$^{2-}$ ions (eq. (4-5)). In the chelate complex, EDTA-$^{2-}$ provided two nitrogen atoms and four oxygen atoms, bringing about the tightly wrapped five-membered chelate rings with high stability. Accordingly, concentration of the free $Ba^{2+}$ ions in the solution was reduced, which slowed the reaction rate.[39] When the slurry derived from the room temperature precipitation was transferred into the stainless steel autoclave for hydrothermal treatment at specific temperature (higher than 130 ºC) for specific time (longer than 6.0 h), the chelate complex EDTA-Ba was gradually decomposed. Subsequently, the gradually released $Ba^{2+}$ ions were combined with $Cl^-$ and $B(OH)_4^-$ ions within the solution, giving rise to the final stabler $Ba_2(B_5O_9)Cl\cdot(H_2O)_{0.5}$ phase,[40-42] as shown in eq. (6).

$$H_3BO_3(s) + H_2O \rightarrow B(OH)_4^-(aq.) + H^+(aq.) \quad (1)$$

$$NaOH\,(aq.) \rightarrow Na^+(aq.) + OH^-(aq.) \quad (2)$$

$$EDTA\text{-}2Na(aq.) \rightarrow EDTA\text{-}^{2-}(aq.) + 2Na^+(aq.) \quad (3)$$

$$BaCl_2(\mathrm{aq.}) \rightarrow Ba^{2+}(aq.) + 2Cl^-(aq.) \quad (4)$$

$$EDTA\text{-}^{2-}\,(\text{aq.}) + Ba^{2+}\,(aq.) \rightarrow EDTA\text{-}Ba(complex) \quad (5)$$

$$4\text{EDTA-Ba(complex)} + 2Cl^{-}\,(\text{aq.}) + 10B(OH)_4^{-}\,(\text{aq.}) + 4H^{+}\,(\text{aq.}) \rightarrow 2Ba_2(B_5O_9)Cl\cdot(H_2O)_{0.5}\,(\text{s}) + 21H_2O + 4\text{EDTA}\text{-}^{2-}\,(\text{aq.}) \quad (6)$$

According to the composition and morphology evolution of the product, the EDTA-2Na assisted formation mechanism of the hierarchical $Ba_2(B_5O_9)Cl\cdot(H_2O)_{0.5}$ microspheres was proposed in **Fig. 5**. Firstly, dissolution of the solid reactants and surfactant EDTA-2Na led to aqueous $B(OH)4^-$, $OH^-$, $Cl^-$ ions and $EDTA^{2-}$ (**Fig. 5(a)**); Secondly, dropping of $Ba^{2+}$ ions into the solution resulted in the coordinate compounds of EDTA-Ba complex due to the strong chelation between $Ba^{2+}$ ions and $EDTA^{2-}$ (**Fig. 5(b)**); Thirdly, room temperature coprecipitation of the aqueous ions and EDTA-Ba complex brought about the nucleation and primary growth of the amorphous NPs with EDTA preferentially adsorbed on the surfaces,[43] when the degree of supersaturation exceeded a certain level (**Fig. 5(c)**); Next, hydrothermal treatment of the above amorphous NPs at specific temperature for specific time promoted the occurrence of $Ba_2(B_5O_9)Cl\cdot(H_2O)_{0.5}$ phase and also increase in the crystallinity as well as self-assembly of the NPs, giving rise to $Ba_2(B_5O_9)Cl\cdot(H_2O)_{0.5}$ microspheres (**Fig. 5(d)**); Thereafter, with the hydrothermal treatment going on, the constitutional NPs exhibited 1D preferential growth parallel to the (101) planes, producing the hierarchical $Ba_2(B_5O_9)Cl\cdot(H_2O)_{0.5}$ microspheres consisted of short nanorod-like sub-units (**Fig. 5(e)**). According to the orthorhombic structure model of $Ba_2(B_5O_9)Cl\cdot(H_2O)_{0.5}$ (**Fig. S2(b)**), the unit cell exhibited distinct anisotropic characteristic. Thus, the intrinsic anisotropic crystal structure of $Ba_2(B_5O_9)Cl\cdot(H_2O)_{0.5}$ played the key role in the transformation from the constitutional NPs to 1D nanorods, similar to the preferential growth of the $MgBO_2(OH)$ nanowhiskers reported in our previous work.[44] And the optimum hydrothermal conditions favored such transformation from the dynamic point of view. Notably however, the existence of surfactant EDTA-2Na was crucial for the self-assembly of the NPs at the early stage of the hydrothermal treatment. Finally, when the reaction time was further elongated, the short nanorod-like sub-units further grew into high aspect ratio nanorods via

traditional Ostwald ripening. The subsequent cooling, washing and drying enabled the final formation of the hierarchical $Ba_2(B_5O_9)Cl\cdot(H_2O)_{0.5}$ microspheres (**Fig. 5(f)**).

As confirmed above, EDTA-2Na played a key role as a chelating and capping agent in the formation of the present $Ba_2(B_5O_9)Cl\cdot(H_2O)_{0.5}$ microspheres, very similar to the soft-template assisted self-assembly of the hierarchical mesoporous $SrCO_3$ microspheres.[45] As known, $EDTA^{2-}$ has four carboxylic groups and two lone pairs of electrons on two nitrogen atoms as binding sites.[46] The carboxyl groups of $EDTA^{2-}$ afford a firm spatial symmetric configuration, limiting the $Ba^{2+}$ within the symmetric regions. Thus, by using EDTA-2Na as surfactant, quasi-spherical amorphous NPs were facilely obtained via the selective adsorption of $EDTA^{2-}$ on the surfaces (**Fig. 3(b), Fig. 5(c)**). The subsequent hydrothermal treatment rendered the evolution from amorphous NPs to primary NPs of $Ba_2(B_5O_9)Cl\cdot(H_2O)_{0.5}$ phase, and further promoted the improvement of the crystallinity and self-assembly of the NPs into $Ba_2(B_5O_9)Cl\cdot(H_2O)_{0.5}$ microspheres, ascribed to the hydrogen bonds, electrostatic gravitation and intermolecular force (**Fig. 5(d)**).[47, 48]

### 3.6 $Tb^{3+}$ doped $Ba_2(B_5O_9)Cl\cdot(H_2O)_{0.5}$ microspheres and luminescent properties

The present $Ba_2(B_5O_9)Cl\cdot(H_2O)_{0.5}$ microspheres were evaluated as potential host material for green-emitting luminescent candidate via rare-earth ions doping, and the effect of $Tb^{3+}$ doping amount on the composition and morphology of the products synthesized at 160 ºC for 6.0 h in the presence of EDTA-2Na were shown in **Fig. S3**. As mentioned previously, uniform $Ba_2(B_5O_9)Cl\cdot(H_2O)_{0.5}$ microspheres were obtained without doping (**Fig. 1**). With the doping molar percentage changing within the range of 1%-10%, all products were well indexed to the $Ba_2(B_5O_9)Cl\cdot(H_2O)_{0.5}$ (JCPDS No. 70-3930) phase, with no other distinct impurities detected (**Fig. S3(a)**). However, the crystallinity of the products tended to be lower with the increase in the doping percentage from 1% to 10%. The change of the morphology and crystallinity of the $Ba_2(B_5O_9)Cl\cdot(H_2O)_{0.5}$ microspheres with the increase

in the doping percentage of $Tb^{3+}$ was attributed to the differences of the ionic radius between the $Tb^{3+}$ (0.092 nm) and $Ba^{2+}$ (0.135 nm) ions.[49] When the $Ba^{2+}$ ion was replaced by $Tb^{3+}$ ion during doping, the crystal structure of $Ba_2(B_5O_9)Cl\cdot(H_2O)_{0.5}$ would have to tune to some extent. This phenomenon has been frequently observed in rare earth doped nanostructures, such as ZnO:$Tb^{3+}$ nanophosphors,[50] $NaYF_4$:Yb/Er[51] and $KYb_2F_7$:$Er^{3+}$ nanocrystals.[52] When the doping molar percentage increased from 1% to 2% and to 4%, the microspheres assembled by small NPs were acquired with distinct spherical or quasi-spherical morphology, however the diameter distribution of which became broader (**Fig. S3(b-d)**). Meanwhile, the constitutional nanorod-like sub-units became short, thick and less. When the doping percentage was as 6%, the profile of the so-called spherical assemblies became irregular or spindle-like (**Fig. S3(e)**). With the doping percentage further increased to 8% and 10%, more and more NPs emerged and self-assembled microspheres disappeared, and the profile of the product assemblies turned to completely nonuniform (**Fig. S3(f-g)**). Thus, doping molar percentage had a remarkable impact on the crystallinity and morphology of the hydrothermal products. This was analagous to phase and size evolution of the doped $NaYF_4$:Yb/Er nanocrystals.[51]

To further shed light on the key role of the surfactant EDTA-2Na in the formation of the hierarchical microspheres, extended control experiment was carried out, *i.e.* doping 6% $Tb^{3+}$ in the absence of the surfactant whereas with other conditions remained unchanged. The hydrothermal product was confirmed as the $Ba_2(B_5O_9)Cl\cdot(H_2O)_{0.5}$ (**Fig. S4(a)**) assembles whereas with dumbbell morphology, accompanied by multitudes of NPs (**Fig. S4(b)**). No distinct microspheres were detected. Compared with the hydrothermal products obtained without the surfactant and without $Tb^{3+}$ doping (**Fig. 4(b)**), morphology of the doped product particles obtained in the absence of the surfactant was farther from the microspheres. Thus, the surfactant EDTA-2Na was crucial for the formation of the hierarchical $Ba_2(B_5O_9)Cl\cdot(H_2O)_{0.5}$ microspheres no mater doped or not. Notably however, competition could be existed between EDTA-2Na and dopant during the hydrothermal formation of the

$Ba_2(B_5O_9)Cl\cdot(H_2O)_{0.5}$ microspheres. The surfactant prevailed over the dopant in the formation of the microspheres with remarkable spherical morphology when the doping amount of $Tb^{3+}$ was kept less than 6% (**Fig. S3(e)**). However, with the further increase in the doping amount, the spherical morphology of the product particles became worse and worse.

**Fig. S5** shows the UV-vis absorption spectra of the $Tb^{3+}$ doped $Ba_2(B_5O_9)Cl\cdot(H_2O)_{0.5}$ microspheres dispersed in DI water. Obviously, for each doping molar percentage from 0 to 10%, no distinct absorption was observed within the detect limitation of the instrument whose working range was 200-900 nm. In other words, all of the absorption spectra were relatively featureless, indicating both the hydrothermally synthesized $Ba_2(B_5O_9)Cl\cdot(H_2O)_{0.5}$ microspheres and $Tb^{3+}$ doped ones of good transparent characteristic from the ultraviolet to the visible regions.

### 3.7 Photoluminescent properties

Photoluminescence excitation (PLE) and photoluminescence (PL) spectra of the $Ba_2(B_5O_9)Cl\cdot(H_2O)_{0.5}$:6%$Tb^{3+}$ phosphors are shown in **Fig. 6(a)**. At the excitation of 230 nm, the PL spectrum obviously demonstrated several broad emission bands which peaked at 493, 548, 589, and 625 nm, due to the typical $^5D_4$-$^7F_J$ (J = 6, 5, 4, and 3) transitions of the $Tb^{3+}$ ion (**Fig. 6(a)**, right).[53-55] The strongest emission peak located at 548 nm was assigned to the $^5D_4$-$^7F_5$ transition of $Tb^{3+}$. Under the emission of 548 nm, the PLE spectrum consisted of one wide excitation bands at 230 nm (**Fig. 6(a)**, left), which was ascribed to the f-f transitions of $Tb^{3+}$. Meanwhile, the $Ba_2(B_5O_9)Cl\cdot(H_2O)_{0.5}$:6%$Tb^{3+}$ phosphors exhibited distinct green luminescence under a ultraviolet ray irradiation (**Fig. 6($a_1$)**). To explore the effects of doping amount on the luminescent properties, the PL spectra of the series of $Ba_2(B_5O_9)Cl\cdot(H_2O)_{0.5}$:x$Tb^{3+}$ (x=0%, 1%, 2%, 4 %, 6%, 8%, 10%) phosphors were also recorded, as shown in **Fig. 6(b)**. Apparently, within the wavelength range of 480-640 nm, the $Ba_2(B_5O_9)Cl\cdot(H_2O)_{0.5}$:6%$Tb^{3+}$ phosphors revealed the strongest emission intensity, compared with other doping molar percentage of $Tb^{3+}$. This was further

manifested by the variation of the emission intensity at 548 nm as a function of the doping molar percentage (**Fig. 6($b_1$)**), which showed the intensity first went up with the $Tb^{3+}$ molar percentage increased from 0% to 6%, and then went down with the further increase in the $Tb^{3+}$ molar percentage thereafter. This might be owing to the concentration quenching effect, similar to the previously reported results.[53, 56, 57] The strong emission of the present $Ba_2(B_5O_9)Cl\cdot(H_2O)_{0.5}$:6%$Tb^{3+}$ phosphors suggested the as-obtained $Ba_2(B_5O_9)Cl\cdot(H_2O)_{0.5}$ microspheres as great potential host material for emitting luminescent candidate via rare-earth ions doping.

## 4. Conclusions

In summary, uniform $Ba_2(B_5O_9)Cl\cdot(H_2O)_{0.5}$ microspheres (diameter: 3.0-5.0 μm) consisted of nanorod-like sub-units have been synthesized via a mild surfactant-assisted hydrothermal process (160 ºC, 6.0 h), by using $H_3BO_3$, NaOH and $BaCl_2\cdot 2H_2O$ as raw materials. Effects of process parameters such as reactant concentration, reaction time, temperature, dosage of surfactant EDTA-2Na were investigated in detail, based on which the EDTA-2Na assisted formation mechanism of the $Ba_2(B_5O_9)Cl\cdot(H_2O)_{0.5}$ microspheres was proposed, in which the EDTA-2Na played the key role in the self-assembly of the microspheres. The $Ba_2(B_5O_9)Cl\cdot(H_2O)_{0.5}$ microspheres exhibited transparent characteristic from ultraviolet to visible range. The as-obtained microspheres were also evaluated as the green-emitting host material via $Tb^{3+}$ doping. Within the experimental doping molar percentage of 0-10% in $Ba^{2+}$, the $Ba_2(B_5O_9)Cl\cdot(H_2O)_{0.5}$:6%$Tb^{3+}$ phosphors demonstrated strongest PL intensity, indicating the as-obtained $Ba_2(B_5O_9)Cl\cdot(H_2O)_{0.5}$ microspheres of great promising host candidate for emitting luminescent material via rare-earth ions doping in light display systems or optoelectronic devices.

**Acknowledgement**

This work was supported by the National Natural Science Foundation of China (No. 21276141). The authors also thank the reviewers for the constructive suggestions on the great improvement of the work.

**References**

1. J. C. Claussen, M. A. Daniele, J. Geder, M. Pruessner, A. J. Makinen, B. J. Melde, M. Twigg, J. M. Verbarg and I. L. Medintz, *ACS Appl. Mat. Interfaces*, 2014, **6**, 17837-17847.

2. H. Z. Guo, X. Liu, Y. H. Hou, Q. S. Xie, L. S. Wang, H. Geng and D. L. Peng, *J. Power Sources*, 2014, **260**, 100-108.

3. F. Lu, W. P. Cai and Y. G. Zhang, *Adv. Funct. Mater.*, 2008, **18**, 1047-1056.

4. J. Bai, X. G. Li, G. Z. Liu, Y. T. Qian and S. L. Xiong, *Adv. Funct. Mater.*, 2014, **24**, 3012-3020.

5. X. H. Rui, H. T. Tan, D. H. Sim, W. L. Liu, C. Xu, H. H. Hng, R. Yazami, T. M. Lim and Q. Y. Yan, *J. Power Sources*, 2013, **222**, 97-102.

6. C. Zhang, L. H. Qian, K. Zhang, S. L. Yuan, J. W. Xiao and S. Wang, *J. Mater. Chem. A*, 2015, **3**, 10519-10525.

7. Q. Q. Zhao, X. L. Deng, M. Ding, L. Gan, T. Y. Zhai and X. J. Xu, *CrystEngComm*, 2015, **17**, 4394-4401.

8. B. Wang, H. B. Wu, L. Yu, R. Xu, T. T. Lim and X. W. Lou, *Adv. Mater.*, 2012, **24**, 1111-1116.

9. Y. X. Zhang, Y. Jia, Z. Jin, X. Y. Yu, W. H. Xu, T. Luo, B. J. Zhu, J. H. Liu and X. J. Huang, *CrystEngComm*, 2012, **14**, 3005-3007.

10. A. M. Chen, P. Gu and Z. M. Ni, *Mater. Lett.*, 2012, **68**, 187-189.

11. Z. Q. Zhang, W. C. Zhu, R. G. Wang, L. L. Zhang, L. Zhu and Q. Zhang, *J. Mater. Chem. A*, 2014, **2**, 19167-19179.

12. W. C. Zhu, X. L. Wang, X. Zhang, H. Zhang and Q. Zhang, *Cryst. Growth Des.*, 2011, **11**, 2935-2941.

13. H. C. Pang, G. L. Ning, W. T. Gong, J. W. Ye, Y. Lin and X. N. Pan, *New J. Chem.*, 2011, **35**, 1449-1452.

14. S. Afyon, D. Kundu, A. J. Darbandi, H. Hahn, F. Krumeich and R. Nesper, *J. Mater. Chem. A*, 2014, **2**, 18946-18951.

15. P. A. Plachinda, V. A. Dolgikh, S. Y. Stefanovich and P. S. Berdonosov, *Solid State Sci*, 2005, **7**, 1194-1200.

16. Y. Z. Huang, L. M. Wu, X. T. Wu, L. H. Li, L. Chen and Y. F. Zhang, *J. Am. Chem. Soc.*, 2010, **132**, 12788-12789.

17. Z. H. Chen, S. L. Pan, Z. H. Yang, X. Y. Dong, X. Su and Y. Yang, *J. Mater. Sci.*, 2013, **48**, 2590-2596.

18. M. M. D. J. Lloyd, A. Levasseur and E. C. Fouassier, *J. Solid State Chem.*, 1973, **6**, 179-186.

19. D. H. Zhu, S. Yun, X. Y. Nai, D. M. Zhao, X. Liu and W. Li, *Cryst. Res. Technol.*, 2013, **48**, 6-10.

20. D. H. Zhu, X. Y. Nai, Q. Q. Song, S. Yun, Y. X. Zhang and W. Li, *Adv. Mater. Res.*, 2012, **535-537**, 2567-2570.

21. P. Held, J. Liebertz and L. Bohaty, *Z. Kristallogr.*, 2002, **217**, 463-464.

22. K. i. Machida, G. y. Adachi, Y. Moriwaki and J. Shiokawa, *Bull. Chem. Soc. Jpn*, 1981, **54**, 1048-1051.

23. C. McMillen, C. Heyward, H. Giesber and J. Kolis, *J. Solid State Chem.*, 2011, **184**, 2966-2971.

24. O. Ferro, S. Merlino, S. A. Vinogradova, D. Y. Pushcharovsky and O. V. Dimitrova, *J. Alloys Compd.*, 2000, **305**, 63-71.

25. J. Brugger, N. Meisser, S. Ansermet, S. V. Krivovichev, V. Kahlenberg, D. Belton and C. G. Ryan, *Am. Mineral.*, 2012, **97**, 1206-1212.

26. T. A. Borisova, O. V. Dimitrova and E. L. Belokoneva, *Crystallogr. Rep.*, 2002, **47**, 390-393.

27. S. Ghose and C. n. Wan, *Am. Mineral.*, 1979, **64**, 187-195.

28. Q. Wei, J. W. Cheng, C. He and G. Y. Yang, *Inorg. Chem.*, 2014, **53**, 11757-11763.

29. E. L. Belokoneva, S. Y. Stefanovich, M. A. Erilov, O. V. Dimitrova and N. N. Mochenova, *Crystallogr. Rep.*, 2008, **53**, 228-236.

30. J. H. Hao and M. Cocivera, *J. Phys.: Condens. Matter*, 2002, **14**, 925-933.

31. J. H. Hao, J. Gao and M. Cocivera, *Appl. Phys. Lett.*, 2003, **82**, 2224-2226.

32. X. M. Zhang, H. Chen, W. J. Ding, H. Wu and J. S. Kim, *J. Am. Ceram. Soc.*, 2009, **92**, 429-432.

33. G. Y. Qu, Z. F. Hu, Y. P. Wang, Q. Yang and L. M. Tong, *Adv. Funct. Mater.*, 2013, **23**, 1232-1237.

34. G. C. Xi, J. H. Ye, Q. Ma, N. Su, H. Bai and C. Wang, *J. Am. Chem. Soc.*, 2012, **134**, 6508-6511.

35. J. Li, S. P. Xia and S. Y. Gao, *Spectrochim. Acta. A. Mol. Biomol. Spectrosc.*, 1995, **51**, 519-532.

36. T. Y. Olson, C. A. Orme, T. Y.-J. Han, M. A. Worsley, K. A. Rose, J. H. Satcher and J. D. Kuntz, *CrystEngComm*, 2012, **14**, 6384-6389.

37. W. Yang, P. Wan, H. Meng, J. M. Hu and L. Feng, *CrystEngComm*, 2015, **17**, 2989-2995.

38. Y. S. Yang, Q. Z. Wu, M. Wang, J. Long, Z. Mao and X. H. Chen, *Cryst. Growth Des.*, 2014, **14**, 4864-4871.

39. J. Geng, F. Jiang, Q. Lu and J. J. Zhu, *CrystEngComm*, 2011, **13**, 2758-2763.

40. L. N. Guo, Y. Z. Wang, Y. H. Wang, J. Zhang and P. Y. Dong, *CrystEngComm*, 2012, **14**, 3131-3141.

41. H. L. Qiu, G. Y. Chen, L. Sun, S. W. Hao, G. Han and C. H. Yang, *J. Mater. Chem.*, 2011, **21**, 17202-17208.

42. I. C. Romero-Ibarra, G. Rodriguez-Gattorno, M. F. Garcia-Sanchez, A. Sanchez-Solis and O. Manero, *Langmuir*, 2010, **26**, 6954-6959.

43. M. H. Lin, H. L. Huang, Z. T. Liu, Y. J. Liu, J. B. Ge and Y. P. Fang, *Langmuir*, 2013, **29**, 15433-15441.

44. W. C. Zhu, S. L. Zhu and L. Xiang, *CrystEngComm*, 2009, **11**, 1910-1919.

45. W. C. Zhu, Z. Z. Liang, X. F. Liu, H. Zhang, Y. J. Zheng, X. L. Piao and Q. Zhang, *Powder Technol.*, 2012, **226**, 165-172.

46. L. Xu, J. M. Shen, C. L. Lu, Y. P. Chen and W. H. Hou, *Cryst. Growth Des.*, 2009, **9**, 3129-3136.

47. R. Li, X. Y. Tao and X. D. Li, *J. Mater. Chem.*, 2009, **19**, 983-987.

48. L. Xu, C. L. Lu, Z. H. Zhang, X. Y. Yang and W. H. Hou, *Nanoscale*, 2010, **2**, 995-1005.

49. R. D. Shannon, *Acta Crystallogr. A*, 1976, **32**, 751-767

50. V. Kumar, S. Som, V. Kumar, V. Kumar, O. M. Ntwaeaborwa, E. Coetsee and H. C. Swart, *Chem. Eng. J.*, 2014, **255**, 541-552.

51. F. Wang, Y. Han, C. S. Lim, Y. H. Lu, J. Wang, J. Xu, H. Y. Chen, C. Zhang, M. H. Hong and X. G. Liu, *Nature*, 2010, **463**, 1061-1065.

52. J. Wang, R. R. Deng, M. A. MacDonald, B. L. Chen, J. K. Yuan, F. Wang, D. Z. Chi, T. S. A. Hor, P. Zhang, G. K. Liu, Y. Han and X. G. Liu, *Nat. Mater.*, 2013, **13**, 157-162.

53. G. Seeta Rama Raju, E. Pavitra and J. S. Yu, *Phys. Chem. Chem. Phys.*, 2014, **16**, 18124-18140.

54. J. Zhou and Z. G. Xia, *J. Mater. Chem. C*, 2014, **2**, 6978-6984.

55. M. M. Jiao, N. Guo, W. Lü, Y. C. Jia, W. Z. Lv, Q. Zhao, B. Q. Shao and H. P. You, *Inorg. Chem.*, 2013, **52**, 10340-10346.

56. J. S. Liao, B. Qiu, H. R. Wen and W. X. You, *Opt. Mater.*, 2009, **31**, 1513-1516.

57. K. Li, M. M. Shang, D. L. Geng, H. Z. Lian, Y. Zhang, J. Fan and J. Lin, *Inorg. Chem.*, 2014, **53**, 6743-6751.

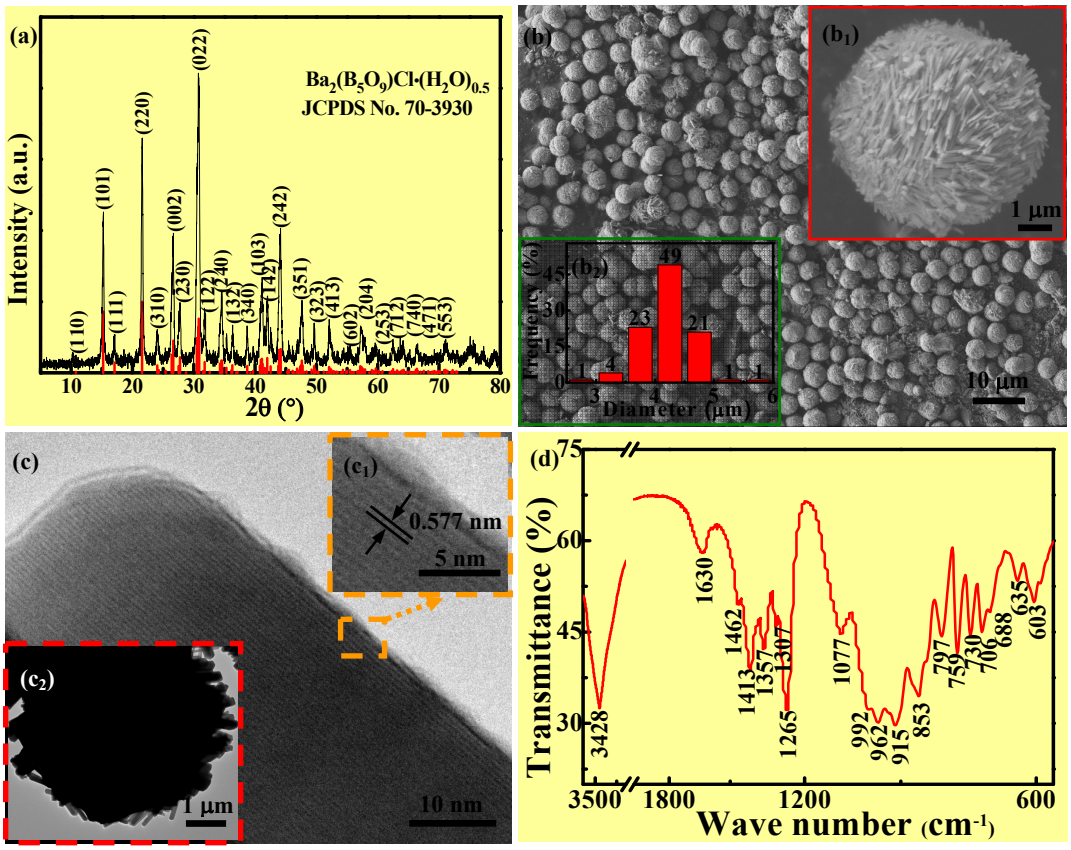


**Fig. 1.** XRD pattern (a), SEM images (b, $b_1$), TEM images (c, $c_2$), HRTEM image ($c_1$), and FT-IR spectrum (d) of the $Ba_2(B_5O_9)Cl{\cdot}(H_2O)_{0.5}$ microspheres hydrothermally synthesized at 160 ºC for 6.0 h, with the molar ratio of Ba:B:OH as 1:2:1, the amount of EDTA-2Na as 8.395 mmol $L^{-1}$ and concentration of $BaCl_2$ as 0.313 mol $L^{-1}$. The inset ($b_1$) and ($b_2$) show a high resolution SEM image and the size distribution of the $Ba_2(B_5O_9)Cl{\cdot}(H_2O)_{0.5}$, vertical lines in (a): the standard pattern of $Ba_2(B_5O_9)Cl{\cdot}(H_2O)_{0.5}$ (JCPDS No. 70-3930).

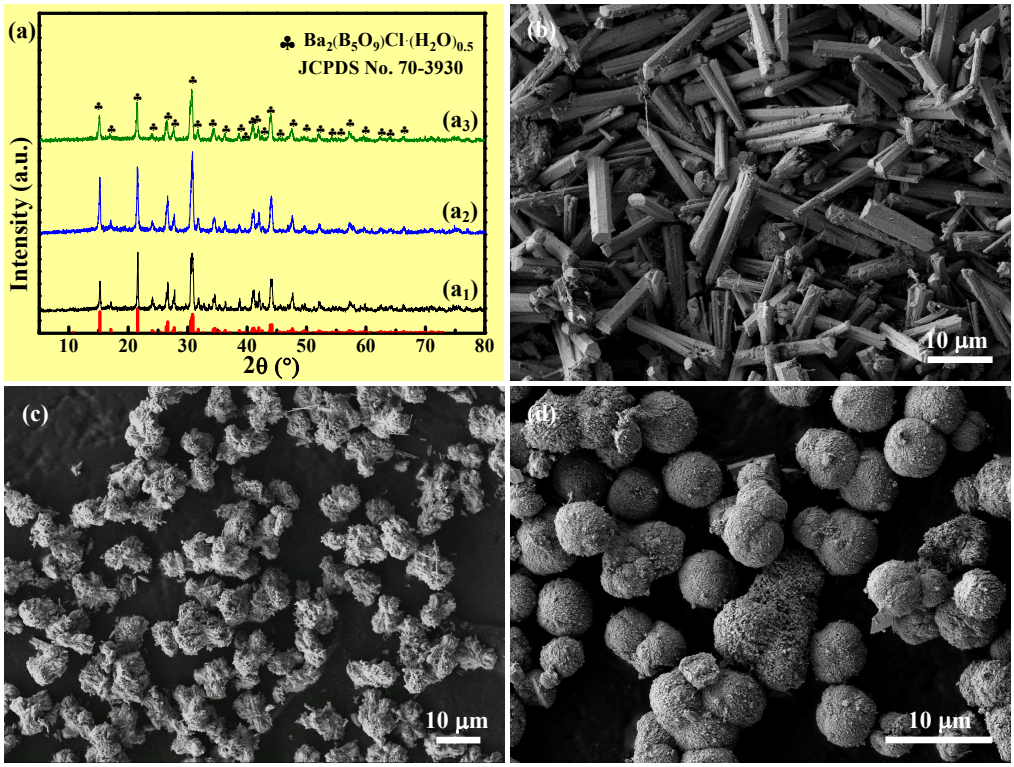


**Fig. 2.** XRD patterns (a) and SEM images (b-d) of the hydrothermal products obtained at 160 ºC for 6.0 h with the molar ratio of Ba:B:OH as 1:2:1, the amount of EDTA-2Na as 8.395 mmol $L^{-1}$ and different reactant concentrations. Concentration of $BaCl_2$ (mol $L^{-1}$): ($a_1$, b)-0.104, ($a_2$, c)-0.209, ($a_3$, d)-0.626.

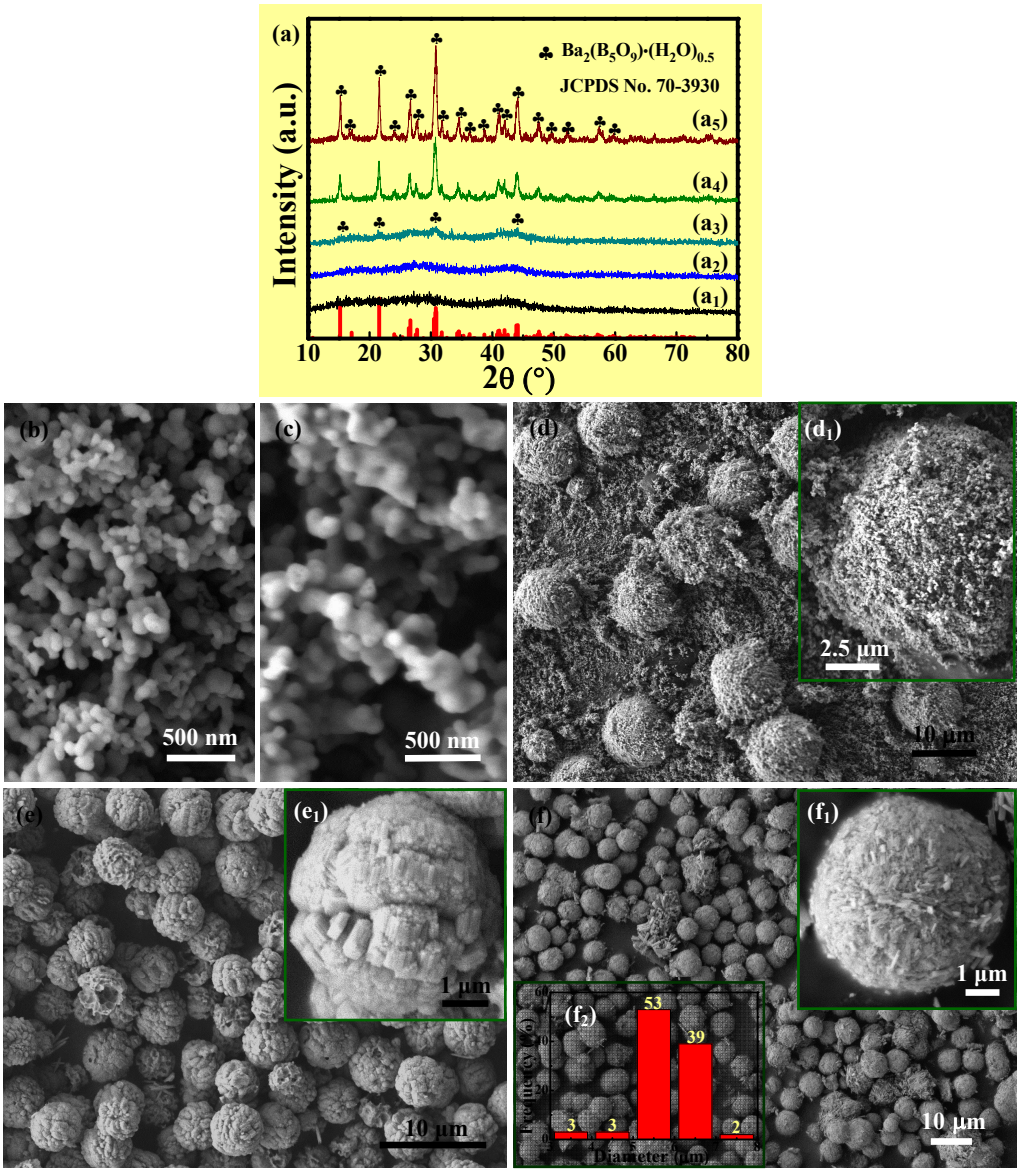


**Fig. 3.** XRD patterns (a) and SEM images (b-f, $d_1$, $e_1$, $f_1$) of the hydrothermal products obtained at different times and temperatures with the molar ratio of Ba:B:OH as 1:2:1, the amount of EDTA-2Na as 8.395 mmol $L^{-1}$ and concentration of $BaCl_2$ as 0.313 mol $L^{-1}$. Time (h): ($a_1$, b)-0.0, ($a_2$, c)-3.0, ($a_3$, d)-6.0, ($a_4$, e)-1.0, ($a_5$, f)-3.0. Temperatue (ºC): ($a_1$, b)-25, ($a_2$, c)-130, ($a_3$, d)-130, ($a_4$, e)-160, ($a_5$, f)-160. The inset ($d_1$-$f_1$) and ($f_2$) show the enlarged SEM images and size distribution of the $Ba_2(B_5O_9)Cl\cdot(H_2O)_{0.5}$ microspheres, respectively.

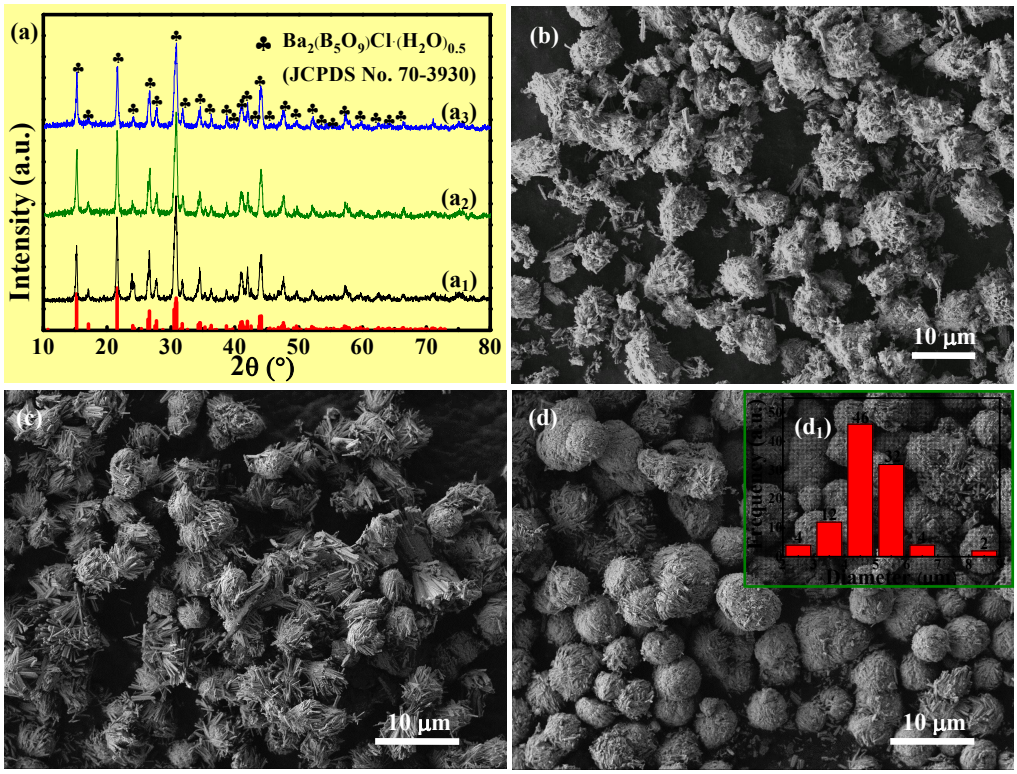


**Fig. 4.** XRD patterns (a) and SEM images (b-d) of the $Ba_2(B_5O_9)Cl·(H_2O)_{0.5}$ microspheres obtained at 160 ºC for 6.0 h with the molar ratio of Ba:B:OH as 1:2:1, initial reactant concentration of $BaCl_2$ as 0.313 mol $L^{-1}$ and different dosage of the surfactant EDTA-2Na. Dosage of the EDTA-2Na (mmol $L^{-1}$): ($a_1$, b)-0.0, ($a_2$, c)-2.798, ($a_3$, d)-16.790. The inset ($d_1$) shows the size distribution of the corresponding $Ba_2(B_5O_9)Cl·(H_2O)_{0.5}$ microspheres.

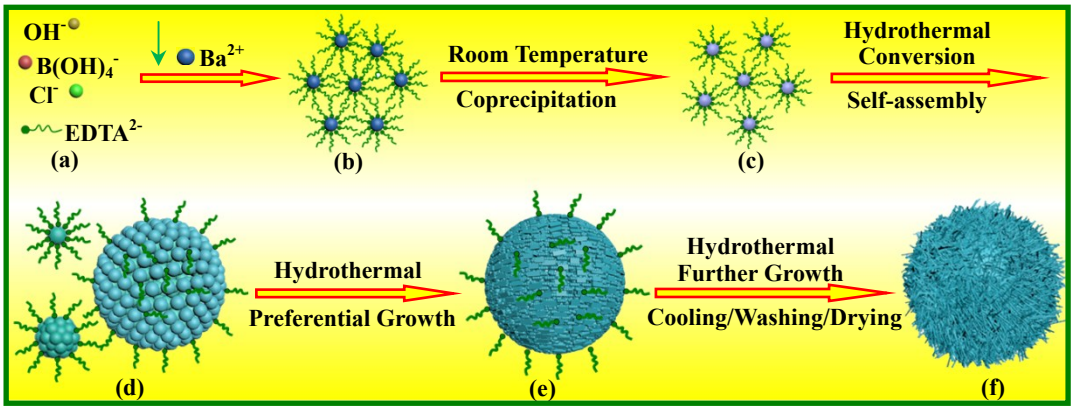


**Fig. 5.** EDTA-2Na assisted formation mechanism of the $Ba_2(B_5O_9)Cl{\cdot}(H_2O)_{0.5}$ microspheres. (a) Dissolution of the solid reactants and surfactant EDTA-2Na led to aqueous $B(OH)4^-$, $OH^-$, $Cl^-$ ions and $EDTA^{2-}$; (b) Dropping of $Ba^{2+}$ into the solution resulted in formation of the coordinate compounds of EDTA–Ba complex; (c) Room temperature coprecipitation of the aqueous ions and EDTA-Ba brought about the nucleation and primary growth of the amorphous NPs; (d) Hydrothermal treatment of the amorphous NPs at specific temperature for specific time promoted the occurrence of $Ba_2(B_5O_9)Cl{\cdot}(H_2O)_{0.5}$ phase and increase in the crystallinity as well as self-assembly of the NPs, giving rise to $Ba_2(B_5O_9)Cl{\cdot}(H_2O)_{0.5}$ microspheres; (e) With the hydrothermal treatment going on, the constitutional NPs exhibited preferential growth, producing the hierarchical $Ba_2(B_5O_9)Cl{\cdot}(H_2O)_{0.5}$ microspheres consisted of short nanorod-like sub-units. (f) When the hydrothermal time was further elongated, the short nanorod-like sub-units further grew into high aspect ratio nanorods via Ostwald ripening, and the subsequent cooling, washing and drying enabled the final formation of the hierarchical $Ba_2(B_5O_9)Cl{\cdot}(H_2O)_{0.5}$ microspheres.

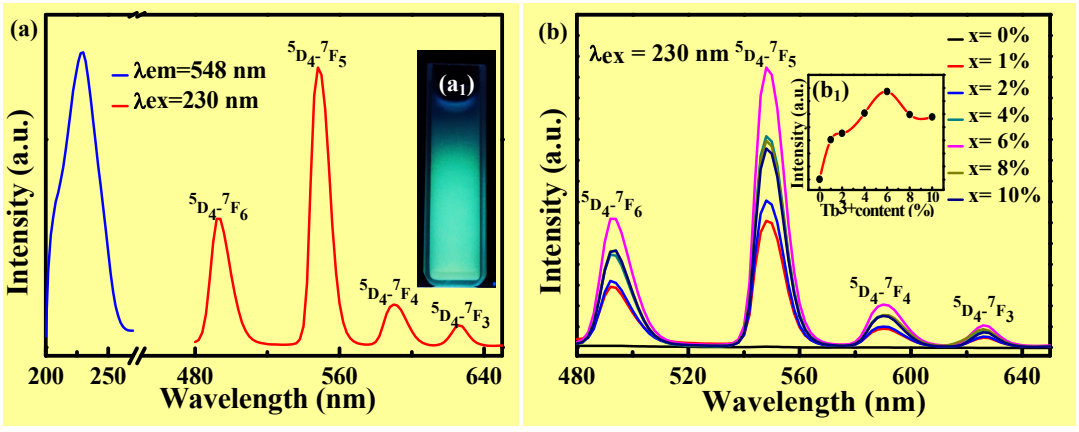


**Fig. 6.** Photoluminescence excitation (PLE) spectrum (λem=548 nm) and photoluminescence emission (PL) spectrum (λex=230 nm) of the $Ba_2(B_5O_9)Cl{\cdot}(H_2O)_{0.5}$:6%$Tb^{3+}$ phosphors (a) as well as emission spectra (λex=230 nm) of the $Ba_2(B_5O_9)Cl{\cdot}(H_2O)_{0.5}$:x$Tb^{3+}$ phosphors with various doping percentage of $Tb^{3+}$ (a). The inset ($a_1$) and ($b_1$) show the green luminescence from the $Ba_2(B_5O_9)Cl{\cdot}(H_2O)_{0.5}$:6%$Tb^{3+}$ phosphors recorded with a digital camera and the variation of emission intensity as a function of doping percentage of $Tb^{3+}$, respectively.